

## Article

# CNN-Based Pattern Classifiers for Precise Identification of Perinatal EEG Biomarkers of Brain Injury in Preterm Neonates

Hamid Abbasi <sup>1,2,\*</sup> , Malcolm R. Battin <sup>3</sup>, Deborah Rowe <sup>3</sup>, Robyn Butler <sup>3</sup>, Alistair J. Gunn <sup>1</sup>  and Laura Bennet <sup>1,\*</sup>

<sup>1</sup> Department of Physiology, Faculty of Medical and Health Sciences, University of Auckland, Auckland 1023, New Zealand; aj.gunn@auckland.ac.nz

<sup>2</sup> Auckland Bioengineering Institute (ABI), University of Auckland, Auckland 1010, New Zealand

<sup>3</sup> Department of Newborn Services, Auckland City Hospital, Auckland 1023, New Zealand; malcolmb@adhb.govt.nz (M.R.B.)

\* Correspondence: h.abbasi@auckland.ac.nz (H.A.); l.bennet@auckland.ac.nz (L.B.)

**Abstract:** Electroencephalographic (EEG) monitoring is important for the diagnosis of hypoxic-ischemic (HI) brain injury in high-risk preterm infants. EEG monitoring is limited by the reliance on expert clinical observation. However, high-risk preterm infants often do not present observable symptoms due to their frailty. Thus, there is an urgent need to find better ways to automatically quantify changes in the EEG these high-risk babies. This article is a first step towards this goal. This innovative study demonstrates the effectiveness of deep Convolutional Neural Networks (CNN) pattern classifiers, trained on spectrally-detailed Wavelet Scalograms (WS) images derived from neonatal EEG sharp waves—a potential translational HI biomarker, at birth. The WS-CNN classifiers exhibit outstanding performance in identifying HI sharp waves within an exclusive clinical EEG recordings dataset of preterm infants immediately after birth. The work has impact as it demonstrates exceptional high accuracy of  $99.34 \pm 0.51\%$  cross-validated across 13,624 EEG patterns over 48 h raw EEG at low 256 Hz clinical sampling rates. Furthermore, the WS-CNN pattern classifier is able to accurately identify the sharp-waves within the most critical first hours of birth ( $n = 8, 4:36 \pm 1:09$  h), regardless of potential morphological changes influenced by different treatments/drugs or the evolutionary ‘timing effects’ of the injury. This underscores its reliability as a tool for the identification and quantification of clinical EEG sharp-wave biomarkers at bedside.

**Keywords:** neonatal EEG; convolutional neural network (CNN); deep learning; pattern recognition; wavelet scalogram image processing; clinical EEG sharp wave; micro-scale neonatal epileptiform seizures



**Citation:** Abbasi, H.; Battin, M.R.; Rowe, D.; Butler, R.; Gunn, A.J.; Bennet, L. CNN-Based Pattern Classifiers for Precise Identification of Perinatal EEG Biomarkers of Brain Injury in Preterm Neonates. *Signals* **2024**, *5*, 264–280. <https://doi.org/10.3390/signals5020014>

Academic Editor: Ran Xiao

Received: 5 February 2024

Revised: 22 March 2024

Accepted: 23 April 2024

Published: 28 April 2024



**Copyright:** © 2024 by the authors. Licensee MDPI, Basel, Switzerland. This article is an open access article distributed under the terms and conditions of the Creative Commons Attribution (CC BY) license (<https://creativecommons.org/licenses/by/4.0/>).

## 1. Introduction

Hypoxic-Ischemic (HI) brain injury due to lack of cerebral oxygen at birth is shown to be followed by a critically short window of opportunity for potential treatments in newborn babies [1,2]. Premature babies are at much higher risks of neurological injury due to HI [3–5]. Uncontrolled Hypoxic-Ischemic Encephalopathy (HIE) evolves from a few hours to days after birth resulting in severe neurodevelopmental impairments, disability, and death [6]. In term neonates, therapeutic hypothermia (TH: brain cooling) can optimally stop the spread of brain damage only if initiated within the very early 2–3 h of birth [7,8]. Conditions are often more complex for preterm infants for whom hypothermia is not applicable, and who seldom exhibit symptoms due to their frailty [9,10]. Hence, there is an urgent need to identify reliable prognostic biomarkers that enable the development of automated strategies for swiftly diagnosing the injury before it becomes irreversible. This will ensure the implementation of the appropriate type of treatment at the right time.

Our post HI monitoring of raw Electroencephalogram (EEG) signals from clinically relevant in utero preterm fetal sheep models has permitted our group to identify the first HI biomarkers in the HI EEG, in the form of micro-scale sharp waves [11–14], which correlate

with injury [13], within the first few hours of HI at 1024 Hz sampled EEG background (refer to Figure 1a,c,d in reference [11]). We have recently demonstrated that translational sharp waves with similar morphology ( $r = 0.94$ ) to those observed in fetal sheep after HI events are also present in the lower 256 Hz sampled clinical EEG of extremely preterm neonates during the first 6 h of life (refer to Figures 1b,e,f, 2 and 3 in reference [11] for visual representations). Unlike experimental models where the start of trial is known, in clinical practice the exact timing of pre-birth HI is unknown and is often challenging to be determined [15]. In other words, the exact time of birth is not necessarily aligned with the time of occlusion, as can be achieved in controlled animal experiments (refer to Figure 1a,b in reference [11] for visual representations). This implies that the brain injury may have already well-evolved beyond the window of opportunity for the available treatments [8,16]. Hence, the necessity of developing reliable automatic algorithms for real-time identification of HI sharp waves, as potential early biomarkers of an evolving HI brain injury [11,13], becomes even more critically important.

Recent advances in machine learning strategies and in particular the use of robust convolutional neural network (CNN) architectures have been beneficial to HI research for the detection of clinical neonatal EEG seizures and grading [17–20] as well as epileptic EEG discharges [21]. However, current automated strategies in clinical HI studies are mostly concerned with determining the degree of HI through classification of EEG segments as well as automatic identification of high amplitude seizures after the window of opportunity has passed [22–26]. From animal studies we know that the high amplitude seizures mark the close of the window of opportunity for treatment (refer to Figure 1a of reference [11]) [15]. Therefore, accurate identification of early signatures of HI brain injury (i.e., micro-scale sharp waves) within the very first hours of birth could provide the opportunity for an effective diagnosis of HI injury and will help to optimize manual interventions.

Our research group has previously reported several successful fusion techniques for the precise identification of sharp wave patterns [11,13,14] and HI gamma spike transients [27] in the HI EEG of preterm fetal sheep, during the early 6–7 h ‘latent-phase’ of the injury post-HI. The wavelet-scalogram CNN structure presented in this work was initially introduced in a preliminary conference paper for the identification of sharp waves in a small experimental dataset of HI EEG of preterm fetal sheep post HI-insult [28]. It has also been tested for the identification of HI gamma spike transients [27]. Furthermore, we demonstrated that a higher number of automatically quantified sharp waves after the first 2 h of HI insult in preterm fetal sheep models is significantly correlated with more subcortical damage [13]. This correlation prompted our interest in investigating this wave-type in preterm human EEG [11].

This article presents, for the first time, the exceptional capabilities of convolutional neural network (CNN)-based pattern classifiers in accurately identifying HI sharp wave biomarkers in a large dataset of 256 Hz sampled EEG from human preterm infants at birth. The work indicates how spectrally-rich wavelet scalograms (WS) of clinical EEG can serve as inputs to a deep 2D-CNN pattern classifier for sharp wave identification. The WS-CNN pattern classifier underwent training using an exclusive data bank of clinical recordings, comprising 6812 EEG sharp waves sampled at 256 Hz clinical sampling rate, from eight preterm infants during their first 6–7 h of life ( $n = 8$ , total of 48 h recording), manually identified by an expert. The performance of the WS-CNN pattern classifier was also assessed against a wavelet-Fourier CNN (WF-CNN), a conventional 1D-CNN, and a wavelet-Fuzzy approach introduced previously in [13,14]. The article outlines how the WS-CNN pattern classifier robustly identifies HI sharp waves from EEG background and artifacts, irrespective of potential morphological changes induced by treatments/drugs. We determined a high cross-validated accuracy of  $99.34 \pm 0.51\%$ , showcasing exceptional performance without the need for manual intervention.

## 2. Data Acquisition

### 2.1. Ethics

The study holds ethics approval from the Health and Disability Ethics Committees (HDEC), New Zealand (ethics number 13/NTB/49).

### 2.2. Clinical Procedures

In this study, we utilized data obtained from a random subset ( $n = 8$ ) of participants enrolled in an observational cohort study involving 33 extremely preterm infants born at  $\leq 28$  weeks estimated gestation at Starship Children's Hospital, Auckland, New Zealand, spanning the years 2014 to 2017. All infants in the cohort received standard clinical and nursing care. The initiation of EEG recordings occurred as soon as possible after birth and extended for a period of 3 days, with a median starting age of 4:36 h (range: 2:45 to 6:32 h). EEG activity was monitored using leads symmetrically placed on the left and right sides of the infant's skull. Recordings were made on the reBRM2 monitor, a research version of the BRM2 manufactured by BrainZ Instruments, Auckland, New Zealand. The EEG signals from both sides were amplified by a factor of 5000 and subjected to filtering using a first-order high-pass filter with a  $-3$  dB frequency at 1 Hz and a fourth-order low-pass Butterworth filter with a  $-3$  dB frequency at 50 Hz. The signal was digitized by the computer at a sampling rate of 256 Hz, and data were continuously collected for 48 h from initiation, with exclusive analysis conducted on recordings obtained during the first 6–7 h after birth.

In this study, only the initial 6 h of EEG data from each neonate were employed for sharp wave analysis. Data from each neonate were selected from either the left or right EEG channel, prioritizing channels with minimal signal corruption. Initially, an expert (HA) manually labeled HI sharp waves in the entire dataset to establish a reliable benchmark for comparison with automatically detected sharp waves.

To ensure the integrity of both clinical care and research activities, experienced neonatal intensive care unit (NICU) nurses, specifically assigned for this project and available in addition to the standard clinical team, placed the EEG electrodes. Instances of physiological instability, drug administration, blood sampling, and routine infant care were documented. Details of antenatal and postnatal treatments, including the administration of sedatives and steroids, were recorded. Infants with congenital or genetic abnormalities, or those with scalp injury/infection, were excluded from the analysis. EEG leads were sited once the infant was stabilised and the first 6 h only of EEG recordings utilised for the current analysis so the exposure to medication was quite limited. Specifically, the majority had received antenatal corticosteroids as per routine practice, antenatal magnesium sulphate was also commonly given and the majority received routine antibiotics with amoxicillin and gentamicin. Surfactant, if required, had typically been administered prior to the start of EEG monitoring. Due to the real world aspects of providing appropriate clinical care to extremely premature infants in the first few hours of life, it is not possible to collect EEG data without prior exposure to drugs such as antenatal steroids and surfactant.

### 2.3. Neonatal HI Micro-Scale Sharp Waves

EEG sharp wave patterns in preterm infants are known to be originated from central and occipital regions [29], typically with amplitudes ranging from 10 to 75  $\mu\text{V}$  around 30 weeks of gestational age. These amplitudes can escalate to higher levels, reaching 260  $\mu\text{V}$  [30] or even 300  $\mu\text{V}$  [29]. Additionally, epileptiform waveforms with lower amplitudes of 10–25  $\mu\text{V}$  have been identified in the EEG of sick preterm human babies [31]. In clinical practice, fast epileptiform events lasting  $<100$  ms (mostly 20–70 ms [32]) are categorized as spike transients, while sharp waves are defined as patterns with durations of 100–200 ms [33]. This definition differs from the conventional one for epileptiform seizures, where events are described as repetitive and rhythmic waves with various frequencies and/or amplitudes lasting for at least 10 s [34].

We have previously demonstrated the ‘translational’ value of micro-scale sharp-wave EEG patterns, characterized by amplitudes between 20–80  $\mu\text{V}$  and durations between 70 and 250 ms, within the latent phase of fetal sheep data [11,13,14,35]. Additionally, we have established their existence during the critical early postnatal period in clinical recordings from profoundly premature neonates within the early hours of birth, making them promising candidates to serve as a reliable marker for HIE [11,13,14,35]. For consistency with our definitions for sheep HI EEG, we define neonatal HI sharp waves in preterms with similar characteristics, superimposed on a suppressed HI EEG background. These patterns occur in the frequency range of 4 to 14.3 Hz, encompassing the  $\theta$  (4–8 Hz),  $\alpha$  (8–12 Hz), and lower-beta  $\beta$  band (i.e., 12–14.3 Hz). Our research indicates that EEG sharp waves hold predictive value for the latent phase of injury following an HI insult. A higher number of sharp waves within the first 30 min post-HI correlates with enhanced subcortical neuronal survival in the caudate nucleus ( $r = 0.8$ ). Conversely, increased sharp-wave activity between 2–4 h after HI is associated with more damage and reduced neuronal survival in the same subcortical region ( $r = -0.83$ ) [13]. These observations underscore the significance of micro-scale EEG waveforms in a suppressed background as early indicators of HIE, emphasizing the need to explore the development of automated methods to accurately capture their presence in bedside monitoring at birth. We refer to these HI micro-scale sharp waves as ‘sharp waves’.

### 3. Related Works

The complex deep learning structures contain a much higher number of artificial nodes and neurons that can better mimic the intricate connectivity of the human brain [36,37]. Literature indicates that 1-dimensional time-series can be directly fed into various formats of CNN architectures for EEG pattern recognition/classification [38,39]. Recent studies demonstrated the utility of mathematical tools in the spectral analysis of EEG [17,40]. Other research shows the capabilities of deep-learning approaches in identifying seizures in neonatal EEG [20,41,42]. A few recent studies have explored the potential of CNNs in the automatic analysis of brain data, addressing tasks such as predicting epileptic seizures [43,44], identifying EEG artifacts [45,46], and detecting high-frequency EEG oscillations [47,48]. However, there is limited research on using CNNs specifically for the identification and classification of seizure-like patterns in EEG [39,49–54]. Most recent literature has primarily focused on employing combinations of spectral features and various CNN structures for the automated identification of neonatal EEG seizures and their correlation with the severity of damage [52,55–58]. Alongside our preliminary conference work utilizing limited fetal sheep data [28], recent research has been focused on identifying clinical EEG biomarkers of HIE in neonatal EEG datasets [19,59–62].

In contrast, the present study offers a comprehensive investigation into the effectiveness of our deep WS-CNN, WF-CNN, and 1D-CNN techniques, each with varying numbers of layers, for identifying sharp-wave EEG patterns across an extensive 48-h clinical dataset from extremely premature infants during their early hours of life.

## 4. Methods

### 4.1. Pre-Processing

The raw EEG from a two-lead electrode system sampled at the clinical sampling rate of 256 Hz was directly used for feature extraction and further analysis. Due to the nature of work, some recordings were quite noisy, and in some cases the datasets were contaminated with more than just the 50 Hz noise. No de-noising of the data was performed such that the WS-CNN pattern classifier performance could be assessed in real-world noisy situations. Therefore, the normalized/zero-measured raw samples were directly used to extract scalogram features.

#### 4.2. Scalogram Image Feature Extraction

A typical sharp wave with a length of 70–250 ms contains spectral components ranging between 4–14.3 Hz (theta and alpha range). The clinical sampling rate of 256 Hz is spectrally rich-enough to capture sharps with a sufficient resolution. We have previously shown that Gaussian 2 mother wavelet (or Mexican hat) holds ideal features which desirably match with inherent spectral characteristics of a HI sharp wave; hence is a preferred basis function for the analysis of sharp wave transients [13,14]. To extract spectral features, this work generates the CWT scalogram images of the EEG sections over a broad scale-range of 1 to 40 using Gaussian 2 mother wavelet at a readable resolution of  $303 \times 404$  pixels. Figure 1A–D illustrate examples of the HI sharp wave transients in the clinical data, taken from the raw neonatal EEGs, post-HI insult, whereas examples of the non-sharp events are demonstrated in Figure 1I–L.

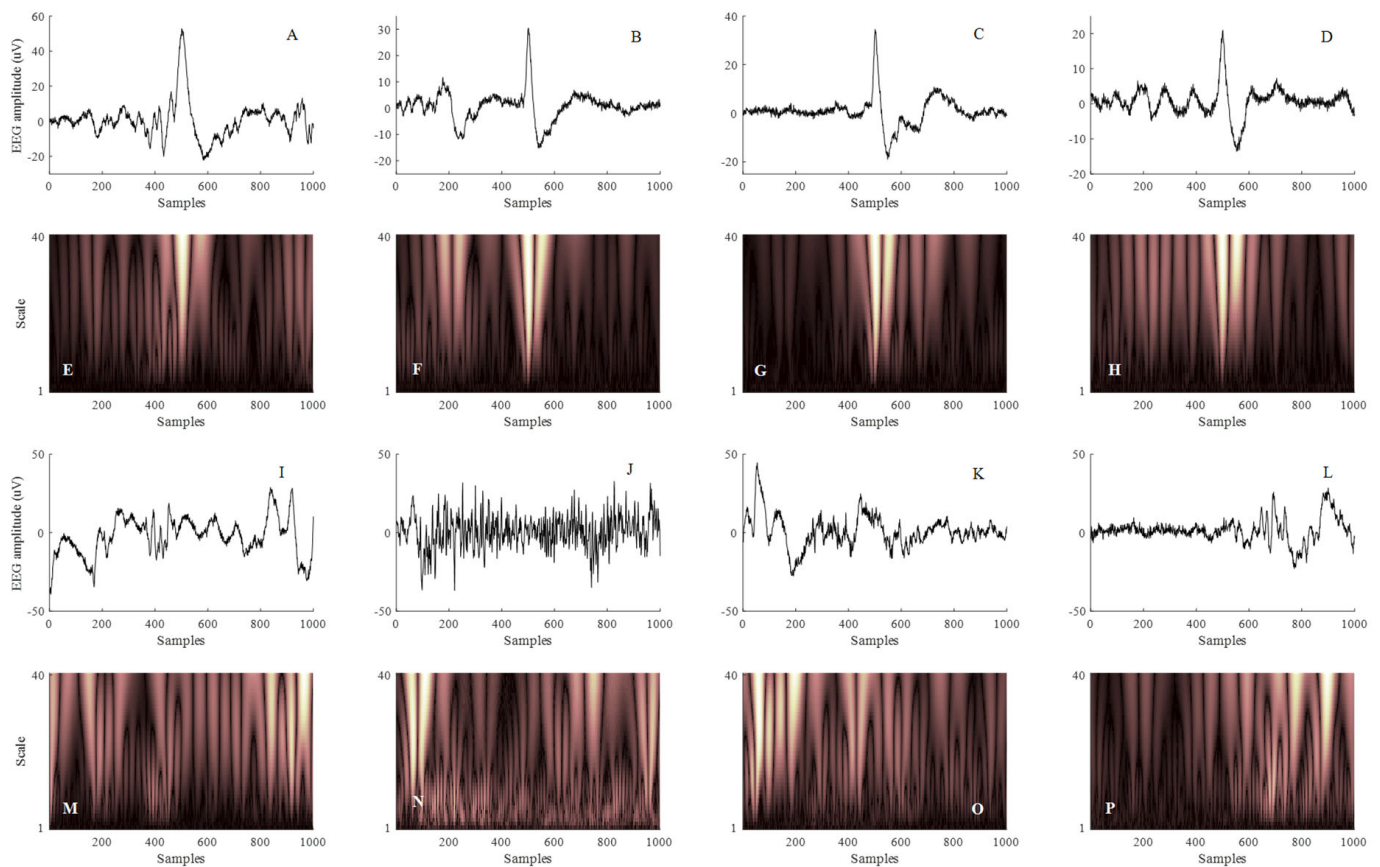


**Figure 1.** Examples of post HI micro-scale sharp waves along profoundly suppressed neonatal EEG in 256 Hz clinical recordings (A–D) as well as non-sharp events (I–L) alongside with their corresponding Wavelet scalograms in (E–H,M–P), respectively, using CWT with Gaus2 basis function of scales 1 to 40. The example wavelet scalogram images in e-h and m-p were used for training, validation and testing of the deep WS–CNN classifier.

The corresponding 2D wavelet scalograms generated from the HI sharp patterns in Figure 1A–D and the non-sharp events in Figure 1I–L are shown in Figure 1E–H and Figure 1M–P, respectively. The illustrations demonstrate how spectrally-rich feature maps of EEG sections can be optimally extracted in the form of high-resolution scalograms images for deep training of a CNN pattern classifier. The WS-CNN pattern classifier was trained on the normalized/zero-meaned raw HI EEG to generalize the performance of the classifier in distinguishing sharp wave patterns from the background EEG and artifact.

#### 4.3. The Deep WS-CNN Classifier: Model Setup and Architecture

This article, in particular, employs a 17-layer deep WS-CNN classifier architecture [28] for the automatic classification of HI sharp wave patterns in neonatal clinical data. In comparison to our preliminary conference work, the WS-CNN classifier here was trained using the CWT scalograms of 256 Hz sampled clinical EEG segments using Gaus2 at scales 1–40 for the identification of the HI sharp wave patterns in 8 preterm neonates. The 2D wavelet scalograms provide spectrally-detailed decomposition representations of EEG patterns (feature maps) allowing the CNN classifier to combine/convolve the elements back to differentiate between a sharp wave and the background activity and/or artifact.

A graphical flow-chart of the developed WS-CNN classifier is demonstrated in Figure 2. The designed architecture of the proposed WS-CNN classifier is detailed in Table 1 and Figure 3. The convolutional parameters of the network (i.e., the stride and kernel size), at each layer, were set accordingly. The 2D wavelet scalogram input images ( $303 \times 404 \times 3$ ) were processed through seven convolutional layers before being passed to a three-layer fully connected block and final softmax and classification layers. The original architecture includes a total of 17 layers deep CNN. Each convolutional layer includes a rectified linear activation unit (ReLU) that is accompanied by a max-pool block. The sizes of the kernel filters at each layer were chosen arbitrarily to derive the adequate amount of features from the data. The stride values were also set to 1 and 2 for the convolution and max-pooling layers, respectively, to adjust the mathematical computations.

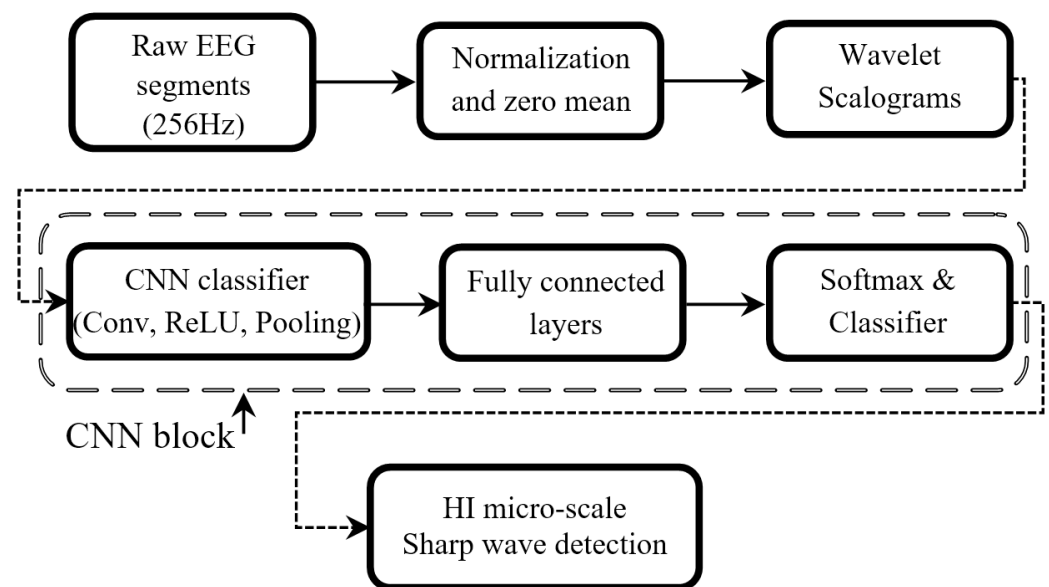


**Figure 2.** The architecture of our proposed WS-CNN classifier.

An original 2D scalogram input of size  $303 \times 404$  was initially passed through seven consecutive convolutional, ReLU, and max-pool layers (each is a convolutional block) and was finally reduced to a much smaller size of  $2 \times 3$ . The number of filters at each convolutional block was set to 16, 32, 48, 72, 96, 128, and 256, respectively. The output of the final max-pool layer was then inserted into a fully connected block with three layers of output size 1536, 24, and 2. The output of the final fully connected layer was then passed into a classification layer for final decision making to choose between a HI sharp wave pattern and a non-sharp segment.

**Table 1.** The Architecture of The Proposed Deep CNN Classifier.

Layers	Type	No. of Neurons (Output Layer)	Kernel Size	Stride	Padding	No. of Filters
0–1	Conv.	$303 \times 404$	3	1	1	16
1–2	Max_pool	$151 \times 202$	[3 2]	2	0	
2–3	Conv.	$151 \times 202$	3	1	1	32
3–4	Max_pool	$75 \times 101$	[3 2]	2	0	
4–5	Conv.	$75 \times 101$	3	1	1	48
5–6	Max_pool	$37 \times 50$	3	2	0	
6–7	Conv.	$37 \times 50$	3	1	1	72
7–8	Max_pool	$18 \times 25$	[3 2]	2	0	
8–9	Conv.	$18 \times 25$	3	1	1	96
9–10	Max_pool	$9 \times 12$	[2 3]	2	0	
10–11	Conv.	$9 \times 12$	3	1	1	128
11–12	Max_pool	$4 \times 6$	[3 2]	2	0	
12–13	Conv.	$4 \times 6$	3	1	1	256
13–14	Max_pool	$2 \times 3$	2	2	0	
14–17	Fully_connected	1536				
	Fully_connected	24				
	Fully_connected	2				
Output	Softmax & Classification					

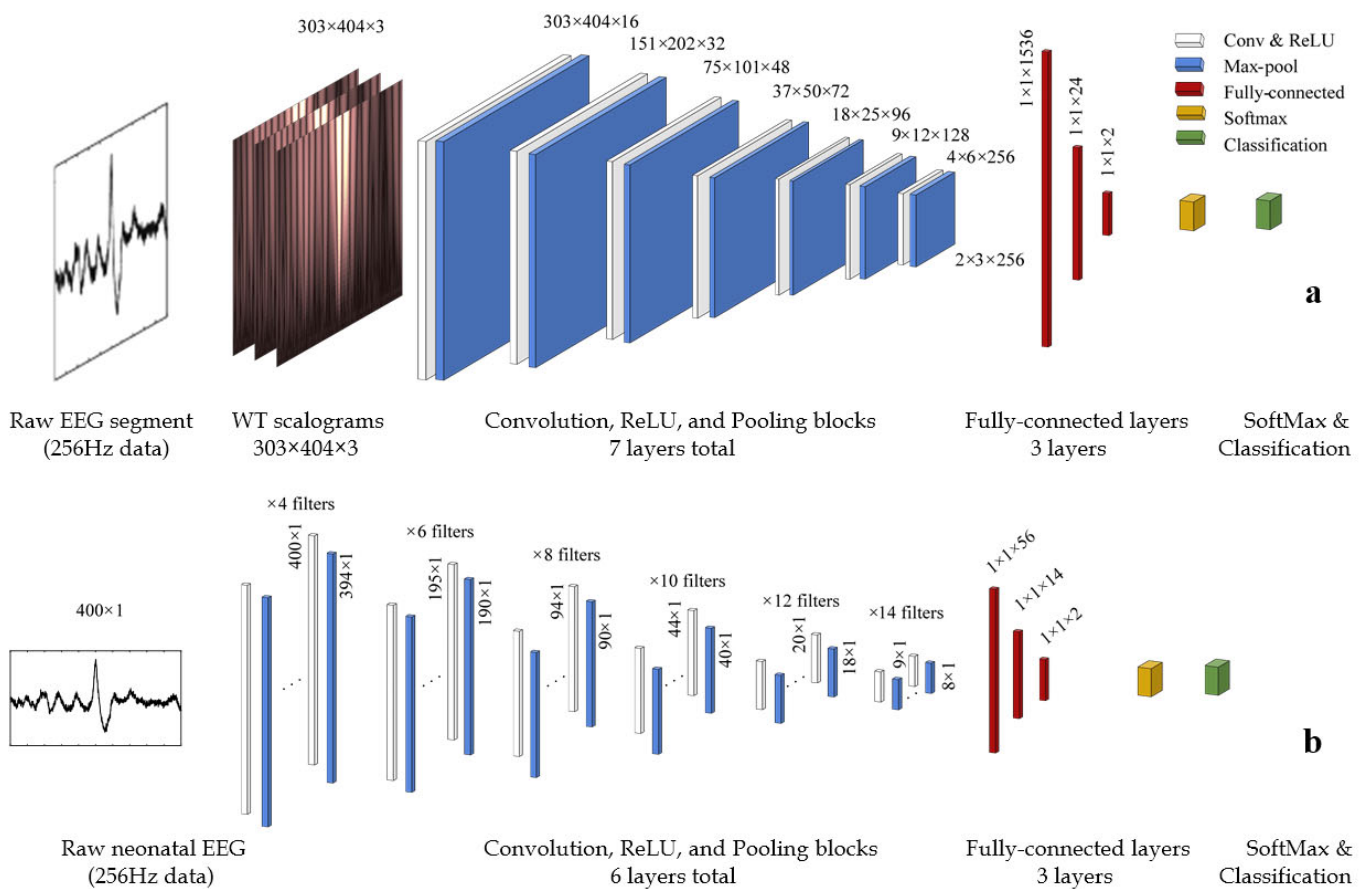


**Figure 3.** The architecture of our proposed (a) WS-CNN and (b) 1D-CNN sharp wave classifiers.

We also investigated reduction of the layer numbers in the proposed WS-CNN architecture. To do so, the original 17 layer structure was re-designed and tested with lower number of layers of 13, 9, and 7 layers. To do so, instead of the seven blocks of convolutional, ReLU, and max-pool layers in the original architecture, we used 5, 3, and 2 blocks in the new architectures. The new architectures were designed only with removing of the convolutional blocks and not with reducing/changing of the size/number of filters in the convolutional blocks. However, the output of the final convolutional block was always designed to match the original size of  $2 \times 3 \times$  corresponding filter size at each layer.

#### 4.4. Computing Infrastructure

The deep WS-CNN pattern classifier were trained using New Zealand eScience Infrastructure (NeSI) high performance computing facilities that offers Cray CS400 cluster. The training process was executed using 12 CPUs (6 hyperthreaded cores) on an Intel Xeon Broadwell node (E5-2695v4, 2.1 GHz) with 18 GB of memory (1.5 GB RAM memory per CPU). The algorithms were developed using MATLAB programming software (version R2023b).

#### 4.5. Training and Testing the WS-CNN Classifier

To minimize the loss function  $E(\theta)$ , a Stochastic Gradient Descent with Momentum (SGDM) strategy was employed to optimize the weights and bias parameters of the classifier.

$$\theta_{l+1} = \theta_l - \alpha \nabla E(\theta_l) + \gamma(\theta_l - \theta_{l-1}) \tag{1}$$

Here,  $\theta$  represents the parameters vector. In this work, initial learning rate,  $\alpha$ , and momentum,  $\gamma$ , parameters of the SGDM algorithm were set at 0.01 and 0.9, respectively. The learning rate,  $\alpha$ , is designed to control the learning speed of the classifier during training. The momentum parameter,  $\gamma$ , in the SGDM updating algorithm, controls the convergence through reducing the oscillations of the parameters during upgrading steps on the steepest descent optimization path. Due to the satisfactory performance results of the classifier, the  $\alpha$  and  $\gamma$  parameters were not further tuned. The batch size parameter was set to 128. The batch size indicates the number of training examples at each training iteration, where a higher chosen batch size value will require more memory space.

Figure 4 represents a schematic of data distribution for training, validation, and testing of the net. A total of 13,624 manually annotated clinical EEG patterns (scalogram images), along a total of 48 h clinical data, including 6812 clinical HI sharp waves and 6812 non-sharp sections were used for training, validation and testing of the deep WS-CNN classifier. The non-sharp EEG sections consist of any EEG segment where the defined sharp wave patterns in Section 2.3 were not present. These sections comprise EEG background signal activity and potential artifacts.

**Table 2.** Results of the Wavelet Scalogram CNN Classifier for Sharp Identification (entire 0–6 h-17 layers).

Trained and Validated on Infant No.	No. of Patterns in the Train-Set	Tested on Infant No.	No. of Patterns in the Test-Set	TP Hits	TN Hits	FP Hits	FN Hits	Sensitivity (%)	Selectivity (%)	Precision (%)	Accuracy (%)
7,9,11,14,17,20,22	10,382	3	3242	1613	1620	1	8	99.5	99.9	99.9	99.7
3,9,11,14,17,20,22	12,274	7	1350	674	664	11	1	99.8	98.4	98.4	99.1
3,7,11,14,17,20,22	11,614	9	2010	1003	1003	2	2	99.8	99.8	99.8	99.8
3,7,9,14,17,20,22	10,818	11	2806	1392	1402	1	11	99.2	99.9	99.9	99.6
3,7,9,11,17,20,22	13,094	14	530	265	260	5	0	100	98.1	98.1	99.1
3,7,9,11,14,20,22	13,176	17	448	224	216	8	0	100	96.4	96.6	98.2
3,7,9,11,14,17,22	12,508	20	1116	553	555	3	5	99.1	99.5	99.5	99.3
3,7,9,11,14,17,20	11,502	22	2122	1060	1059	2	1	99.9	99.8	99.8	99.9
Overall performance of the 17 layers WS-CNN in the entire 0–6 h											99.34 ± 0.51

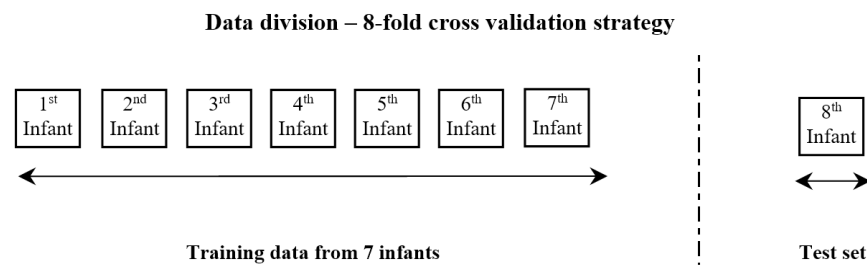


**Figure 4.** Allocations of the EEG datasets for training, validation and testing of the proposed WS-CNN classifier (also see Table 2).

The net was trained over a total of 120 epochs, where each epoch is the presentation of the whole training set to the net, taking almost 66 h to train using the described core configuration in the computing facilities. The entire training datasets were split up into 80% and 20% for training and validation, respectively. The dataset from the remaining unseen infant, which was not used in the training process, was allocated for testing of the net. Finally, substituting the SGDM optimizer with the Root Mean Square Propagation (RMSProp) and Adam updating algorithms resulted in more convergence fluctuations and a much slower training process, respectively, hence these updating algorithms were not investigated further.

#### 4.6. WS-CNN Classifier

The superior compatibility of Gaussian 2 basis function for sharp wave analysis in comparison to other wavelet basis functions would allow to aim for minimal features from a sharp wave to be used in a 2D-CNN. In this approach, instead of the full-range spectral features (scalograms) in the WS-CNN approach, only the spectrally-dominant features of an arbitrary EEG epoch are directly extracted from the raw recordings to form an input set. The CWT coefficients of each zero-meaned EEG segment ( $400 \times 1$ ) using Gaus 2 at scale 32 as well as the inverse Fourier transform time-series of the data (IFFT-spectral components within 4–12.5 Hz were preserved) along with the original raw EEG segment, were combined to create the input-matrix of size  $400 \times 3 \times 1$  to be fed into the deep 2D-CNN classifier (Figure S6 in Supplementary Materials). Compared to the WS-CNN, here the 17 layers 2D WF-CNN classifier is computationally more efficient due the much simpler input-matrix of features, instead of the computationally-intensive scalograms. In fact, the scalograms in Figure 3a are replaced with input-matrix of size  $400 \times 3 \times 1$  containing the CWT, IFFT and the raw EEG data (Figure 3, and Figure S6 and Table S4 in Supplementary Materials). Similar to the WS-CNN, a SGDM updating strategy was used for 8-fold cross-validation of the WF-CNN. Using the procedure described for WS-CNN pattern classifier, the article investigates the effects of reducing the original 17-layer 2D-CNN structure down to 13, 9, and 7 layers by using 7, 5, 3 and 2 blocks of convolutional, ReLU, and max-pool layers in each architecture, respectively.

#### 4.7. 1D-CNN Classifier

Here we investigate the performance of a 1D-CNN classifier where a HI EEG time-series of length  $400 \times 1$  (for both sharp waves and non-sharp events) was directly passed, as the input, to a 15-layer deep 1D-CNN structure for classification. In the 1D-CNN structure, the WS generating block in Figure 2 is by-passed from the previously detailed WS-CNN pattern classifier. The designed architecture of the proposed 1D-CNN pattern classifier is detailed in Figure 3 and Table S5 of Supplementary Materials. The maximum depth of 15-layers was designed, inevitably, based on the limited length of the input EEG segment and considering a stride value of 2 for all max-pooling layers. Using the procedure described for WS-CNN pattern classifier, the article investigates the effects of reducing the original 15-layer 1D-CNN structure down to 13, 9, and 7 layers by using 6, 5, 3 and 2 blocks of convolutional, ReLU, and max-pool layers in each architecture, respectively.

#### 4.8. Wavelet Type-II Fuzzy Classifier

In 2016, we previously developed a successful Wavelet-Type-II-FLC classifier approach that demonstrated ability in the identification of HI sharp waves across data from five preterm fetal sheep with ~97% and ~94% accuracy for the original 1024 Hz and down-sampled 64 Hz data [13,14]. Here we re-investigate the performance of the wavelet-Type-II-FLC method over a more challenging clinical neonatal dataset sampled at a lower 256 Hz resolution. Results of the Wavelet-Type-II-FLC approach will be compared with the accuracy of the WS-CNN and 1D-CNN pattern classifiers. To avoid repetitive content, detailed information on the Wavelet-Type-II-FLC classifier is available in [14]. The high-performance results of this approach using data from preterm sheep were highly related to the fact that: post HI sharp waves emerge analogously with uniform profiles along the suppressed EEG in the experimental data, in the absence of noise contamination. It is assumed that this could get influenced by the high-level of variations/complexity in the clinical EEG.

#### 4.9. Performance Evaluation Metrics

##### (1) K-fold cross-validation for the deep CNN-based classifiers

The performances of the WS-CNN, WF-CNN and 1D-CNN classifiers were evaluated using an eight-fold cross-validation over datasets from eight preterm neonates. Typically, k-fold cross validation is used within a single dataset where the entire dataset is sub-partitioned. Here as in our previous works, in [14,27], we perform cross-validation across 8 infants dataset where the data from each 7 infants represents a sub-partition for training and validation while data from an unseen infant is used for testing of the classifier. Results of the 8-fold cross-validation [63] could implicitly specify whether there is a significant variation in the profile of the HI sharp waves (assumed to be caused by drugs/treatments) across all babies. In other words, training of the networks over k-1 babies (seven) and testing that on the data from an unseen infant (one infant only) could determine the degree of reliability of the proposed pattern classifiers in the identification of HI sharp waves (Figure 4 and Table 2). This cross-validation procedure was repeated eight times across data from eight babies by swapping the test dataset at each time. The reported performance metrics in this article, including sensitivity, selectivity, precision, and overall accuracy measures, are the average of the values (mean  $\pm$  std) calculated from eight evaluations. To assess the reliability of the classifier, the performance of the net was evaluated through two different strategies:

*Performance evaluation over the entire six hours clinical EEG across all eight babies (total of 48 h recordings):* In this approach, data from the entire 6 h of seven babies (42 h) were used for training and validation of the net and data from the entire 6 h of the remaining infant was used to test the classifier. This approach was permuted in a similar manner across all eight babies (8-fold cross-validated) and provides a larger scale performance evaluation over much larger datasets. This approach was also further assessed by investigating the effects of reducing the number of convolutional layers on the overall performance of the classifier.

*Performance evaluation over data from three EEG sub-sections of 2 hourly windows during the first hours of recordings:* This strategy has some benefits that allow for potential matching between early hours of neonatal EEG and post HI experimental recordings. However, birth is not necessarily aligned with the time of insult in our fetal sheep HI experiments, and HI could often happen pre-birth in the womb. In other words, we do not know if the babies have been exposed to hypoxia (or if they have, then to what extent). Also, complexities around the time of birth for preterm babies (i.e., resuscitation) might have caused delays in the initiation of the recordings. Thus, the chosen early 6 h from clinical data does not mimic the reported latent phase in our animal experiments. Moreover, many of the babies receive drugs/special treatments, which we would have assumed causing profile change of the epileptiform seizure-like events within the early hours from birth (i.e., HI micro-scale sharp waves). Therefore, dividing the first 6 h recordings into 2 h sub-windows will help

to assess the performance of the WS-CNN pattern classifier over smaller windows and to check if there is a drop in the overall performance due to the variations in the profile.

(2) K-fold cross-validation for the Wavelet-Type-II-FLC

The performance of the WT-Type-II-FLC classifier approach was also assessed using measures from the 8-fold cross-validation strategy as described in [14]. The WT transformed “footprint of uncertainty” (FOU) profiles of the actual sharp waves, from 7 babies excluding one at each set, were used to identify the sharp waves within the entire 6 h EEG of the remaining unseen infant (i.e., infant #3) (Figure S9i–p of Supplementary Materials).

5. Results

5.1. Cross Dataset Results of the WS-CNN Classifier

Table 3 compares the performance results of the proposed classifiers in the current article. The consistent high performance result of  $99.34 \pm 0.51\%$  across 6 h windows from several babies confirms the reliability of the developed WS-CNN classifier for the identification and classification of the HI sharp wave patterns in the 256 Hz clinical EEG. Results of the confusion matrix from 8-fold cross-validation in Table 3 indicate high sensitivity, selectivity, and precision measures of  $99.66 \pm 0.35\%$ ,  $98.97 \pm 1.17\%$ , and  $99.00 \pm 1.12\%$ , respectively, using data from the entire 6 h EEG recordings across all eight babies. Also, consistent high performances of 98.5–99.1% obtained from the shorter 2-h windows, over the first 0–2 h, 2–4 h, 4–6 h sections of each infant (Tables S6–S8 of Supplementary Materials), confirming the considerable capability of the developed pattern classifier. The classifier was able to desirably identify sharp waves regardless of their positive or negative polarity. In our preliminary work, we had previously estimated that the proposed WS-CNN classifier would be able to perform well on the 256 Hz clinical data through testing of the classifier over 256 Hz down-sampled recordings from the original 1024 Hz animal EEGs [28]. Therefore, results of the current work from the actual 256 Hz clinical datasets validate the previously reported estimations.

**Table 3.** An Illustrative Comparison Between the Evaluated Performances of the Proposed Strategies in the Current Article.

Strategy	No. of Layers	Sensitivity (%)	Selectivity (%)	Precision (%)	Accuracy (%)
WS-CNN	17-layers	$99.66 \pm 0.35$	$98.97 \pm 1.17$	$99.00 \pm 1.12$	$99.34 \pm 0.51$
	13-layers	$99.61 \pm 0.30$	$98.65 \pm 1.54$	$98.69 \pm 1.48$	$99.14 \pm 0.65$
	9-layers	$98.98 \pm 1.13$	$98.35 \pm 0.94$	$98.38 \pm 0.92$	$98.73 \pm 0.87$
	7-layers	$98.13 \pm 1.30$	$97.50 \pm 2.29$	$97.56 \pm 2.19$	$97.81 \pm 1.29$
WF-CNN	17-layers	$98.22 \pm 0.89$	$98.28 \pm 1.44$	$98.32 \pm 1.38$	$98.26 \pm 0.87$
	13-layers	$99.47 \pm 1.22$	$96.83 \pm 3.21$	$96.93 \pm 2.93$	$96.65 \pm 1.46$
	9-layers	$95.70 \pm 1.49$	$95.90 \pm 1.74$	$95.94 \pm 1.64$	$95.81 \pm 1.10$
	7-layers	$94.82 \pm 3.34$	$95.07 \pm 2.74$	$95.19 \pm 2.54$	$94.95 \pm 1.08$
1D-CNN	15-layers	$95.18 \pm 4.79$	$95.30 \pm 2.27$	$95.34 \pm 2.14$	$95.25 \pm 2.10$
	13-layers	$95.81 \pm 4.25$	$97.67 \pm 1.41$	$97.62 \pm 1.36$	$96.75 \pm 2.18$
	9-layers	$88.21 \pm 4.43$	$91.35 \pm 3.89$	$91.21 \pm 3.75$	$89.77 \pm 2.70$
	7-layers	$89.03 \pm 8.55$	$80.63 \pm 12.1$	$83.30 \pm 7.87$	$84.81 \pm 4.34$
WT-Type-II-FLC	Not applicable	$93.03 \pm 2.46$	$58.26 \pm 9.07$	Not applicable	$75.64 \pm 5.31$

We also investigated the effects of reducing the original depth of 17 layers (14 convolutional layers) down to 13, 9 and 7 layers (corresponding to 10, 6 and 4 convolutional layers, respectively), using 8-fold cross-validation over the entire 6 h data across all babies (48 h total). This provided overall accuracies of  $99.14 \pm 0.65\%$ ,  $98.73 \pm 0.87\%$ , and  $97.81 \pm 1.29\%$  for the 13, 9 and 7 layers structures, respectively, while the median value of

the 17 layers structure was higher than other architectures (Figure 5i, also Tables S9–S11 in Supplementary Materials). Results indicated a fair reduction in the total accuracy of the net, while standard deviation increases as the number of layers decreases (Figure 5i). Also, the accuracy reduction using the lower number of layers in Figure 5i includes outliers that highlight much less accurate results in some of the babies. The ROC curves and the corresponding AUC values in Figure 5a–h provide visualization on how the performance of the WS-CNN classifier change across eight babies as the number of layers decreases. It is assumed that the slight reduction in the overall performance using a lower number of convolutional layers is due to the fine-tune/design of the inner convolutional layers in the smaller architectures. In other words, the image size reduction in the smaller network architectures was carefully re-designed to avoid huge image size reductions. Results of the WS-CNN classifier is still higher and much more reliable compared to our previous algorithms for the identification of HI sharp waves in sheep models.

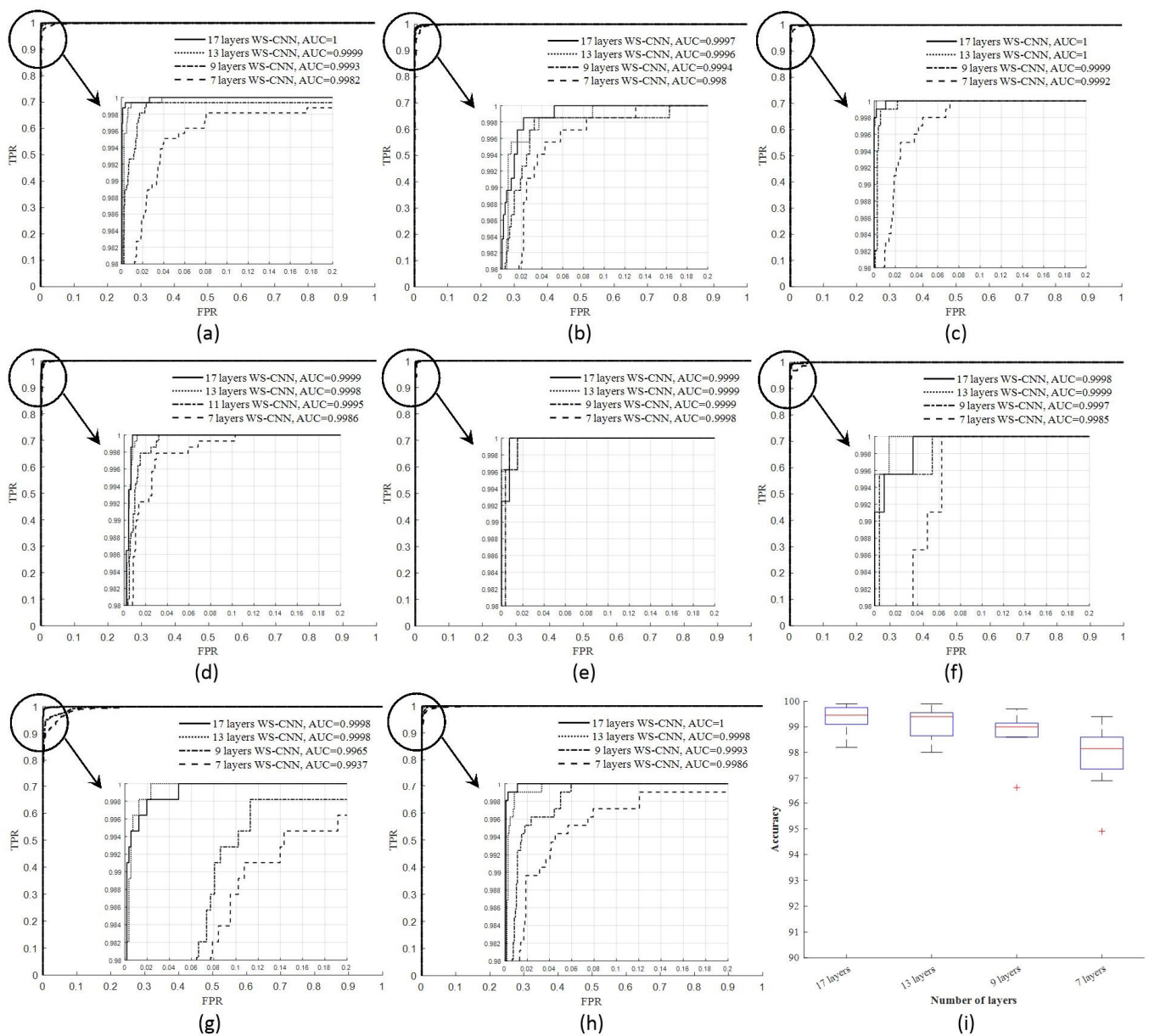


**Figure 5.** (a–h): ROC curves and the corresponding AUC values from 8-fold cross-validation of the results along 6 h of 256 Hz data across 8 babies (48 h total) using 17, 13, 9 and 7 layers in the proposed WS-CNN classifier. The boxplot in (i) demonstrates the overall accuracy of the classifier as the number of layers decreases.

### 5.2. Cross Dataset Results of the WF-CNN Classifier

The 8-fold cross-validated performance validation of the 17-layers WF-CNN pattern classifier resulted in an overall accuracy of  $98.26 \pm 0.87\%$ , tested across 6 h EEG windows of all babies (48 h total). Reducing the original depth of 17-layers WF-CNN architecture (14 convolutional layers) down to 13, 9 and 7 layers (corresponding to 10, 6 and 4 convolutional layers, respectively) resulted in overall accuracies of  $96.65 \pm 1.46\%$ ,  $95.81 \pm 1.09\%$ , and  $94.95 \pm 1.08\%$ , respectively (Table 3). Results of the 17 layers WF-CNN classifier performed better among all architectures. However, the maximum accuracy of the WF-CNN, obtained from the 17-layers architecture was slightly lower than the maximum accuracy of the 17-layers WS-CNN approach. Moreover, the performance of the smallest WF-CNN structure with 7-layers was not considerably lower compared to the smallest WS-CNN. Results of the confusion matrix as well as ROC curves and the corresponding AUC values of the WF-CNN classifier are represented in (Tables S12–S15 and Figure S7 in Supplementary Materials). Compared to the WS-CNN approach, results indicate that the WF-CNN pattern classifier is slightly less efficient in identifying the sharp wave patterns. However, it provides rich-enough features for the 2D-CNN to build feature maps for acute classification which allows user to choose a technique based on their analytical needs.

### 5.3. Cross Dataset Results of the 1D-CNN Classifier

The 8-fold cross-validated performance validation of the 15-layers 1D-CNN pattern classifier resulted in an overall accuracy of  $95.25 \pm 2.10\%$ , tested across 6 h EEG windows of all babies (48 h total). Reducing the original depth of 15-layers 1D-CNN architecture (12 convolutional layers) down to 13, 9 and 7 layers (corresponding to 10, 6 and 4 convolutional layers, respectively) resulted in overall accuracies of  $96.75 \pm 2.18\%$ ,  $89.78 \pm 2.69\%$ , and significantly dropped down to  $84.81 \pm 4.34\%$ , respectively (Table 3). Results indicate that the 13-layers 1D-CNN pattern classifier performed better among all architectures, which indicates that a higher number of layers in this approach does not necessary associate with higher performances.

However, the maximum accuracy of the 1D-CNN, obtained from the 13-layers architecture was still lower than the minimum accuracy of the WS-CNN approach obtained from a 17-layers architecture. Moreover, the performance of the smallest 1D-CNN structure with 7-layers was considerably lower compared to the smallest WS-CNN and WF-CNN architectures with similar number of layers. Results of the confusion matrix as well as ROC curves and the corresponding AUC values of the 1D-CNN classifier are represented in (Tables S16–S19 and Figure S8 in Supplementary Materials). Compared to the WS-CNN and WF-CNN approaches, results in Tables S16–S19 and Figure S8 indicate that the 1D-CNN pattern classifier is much less tolerant in dealing with complex (and often noisy) raw EEG in some babies. The considerable increase in the number of FP and FN hits in Tables S16–S19 reflects this fact.

### 5.4. Cross Dataset Results of the WT-Type-II-FLC

The degree of similarity of the wavelet transformed FOU profiles in Figure S9 of Supplementary Materials infer that the WT-Type-II-FLC classifier must result in desirable high performances. However, the overall performance of the wavelet-fuzzy approach was assessed with a significant drop down to  $75.64 \pm 5.31\%$  with sensitivity and selectivity measures of  $93.03 \pm 2.46\%$  and  $58.26 \pm 9.07\%$ , respectively (Table 3). Table S20 in Supplementary Materials represents the cross-validation results of the WT-Type-II-FLC classifier. In fact, the significant fall in the selectivity measure caused the overall performance of the classifier to drop dramatically, while the sensitivity measure remained roughly high. In general, a lower number of FP and FN hits are aimed for an accurate classifier. Table S20 demonstrates that the WT-Type-II-FLC approach has the ability to pick up on the manually labeled sharp waves (correct detections) with fewer FN hits (missing hits), causing the overall sensitivity to remain high. However, the WT-Type-II-FLC classifier seems to be detecting so many other background transients along the way, causing an increase in the

number of FP hits (wrong detections), which has significantly reduced the selectivity measure, subsequently. Technically, this was expected due to the significant signal variations in the clinical EEG and the level of similarity between wavelet transform of many background EEG rhythms in the theta and alpha wave-range and WT of the desired HI sharp waves. The increase in the standard deviation in the overall performance of the WT-Type-II-FLC classifier can confirm the statement above and can be related to the natural variance in the datasets across data from eight babies.

## 6. Conclusions

This article highlights the exceptional capabilities of convolutional neural network (CNN)-based pattern classifiers, fed with high-resolution wavelet scalogram feature maps, in accurately identifying HI sharp wave biomarkers in a large dataset of 256 Hz sampled EEG from human preterm infants at birth. The remarkable classification accuracy of  $99.34 \pm 0.51\%$  has an impact by indicating the considerable ability of the classifier in the identification of translational sharp wave EEG patterns in the challenging clinical sampling frequency of 256 Hz within the most clinically important first hours of life. The proposed classifier was tested over 13,624 wavelet scalogram images along 48 h of raw EEG data and was able to accurately identify patterns regardless of the type of treatment or drug that the babies had received (this was originally assumed to highly influence the morphology of the patterns, highly). It was shown that the WS-CNN pattern classifier outperforms the WF-CNN, the conventional 1D-CNN and wavelet-fuzzy approaches. Overall, whilst the WS-CNN performs best among all, the other purposed techniques come very close within the error margin, allowing user to choose a strategy based on their computational requirements. The introduced automatic strategy is a big step ahead toward early diagnosis of HI injury in at-risk infants, at bed-side, through real-time identification of EEG biomarkers at birth, where therapeutic protocols have been shown to be optimally neuroprotective in. Signal processing-wise, the introduced method is quite generic and can be re-designed for various applications in many different fields.

**Supplementary Materials:** The following supporting information can be downloaded at: <https://www.mdpi.com/article/10.3390/signals5020014/s1>.

**Author Contributions:** Conceptualization, H.A., L.B., A.J.G. and M.R.B.; Methodology, H.A., L.B., A.J.G., M.R.B., R.B. and D.R.; Software, Validation, Algorithms Development, Manual Annotation, and Formal analysis, H.A.; Investigation, L.B., A.J.G., M.R.B. and R.B.; Resources, H.A., L.B., A.J.G. and M.R.B.; Data curation, H.A.; Writing—original draft, H.A.; Writing—review and editing, H.A., L.B., A.J.G. and M.R.B.; Visualization, H.A.; Supervision, L.B. and A.J.G.; Funding acquisition, L.B. and A.J.G. All authors have read and agreed to the published version of the manuscript.

**Funding:** This research was funded by the Health Research Council of New Zealand. Grant numbers: HRC 17/601, HRC 18/225, and HRC 22/559.

**Data Availability Statement:** The original contributions presented in the study are included in the article/Supplementary Materials, further inquiries can be directed to the corresponding author/s. The raw data supporting the conclusions are unavailable due to ethical restrictions.

**Acknowledgments:** The research was supported by grants from the Health Research Council of New Zealand (HRC-17/601, HRC 18/225, and HRC 22/559). The authors would also like to acknowledge the use of the New Zealand eScience Infrastructure (NeSI) high-performance computing facilities for the results of this research. URL: <https://www.nesi.org.nz> (access date: 20 April 2024).

**Conflicts of Interest:** The authors declare no conflicts of interest.

## References

1. Merchant, N.; Azzopardi, D. Early predictors of outcome in infants treated with hypothermia for hypoxic–ischaemic encephalopathy. *Dev. Med. Child Neurol.* **2015**, *57*, 8–16. [[CrossRef](#)] [[PubMed](#)]
2. Aridas, J.D.; Yawno, T.; Sutherland, A.E.; Nitsos, I.; Ditchfield, M.; Wong, F.Y.; Fahey, M.C.; Malhotra, A.; Wallace, E.M.; Jenkin, G.; et al. Detecting brain injury in neonatal hypoxic ischemic encephalopathy: Closing the gap between experimental and clinical research. *Exp. Neurol.* **2014**, *261C*, 281–290. [[CrossRef](#)] [[PubMed](#)]

3. Parikh, P.; Juul, S.E. Neuroprotection strategies in preterm encephalopathy. *Semin. Pediatr. Neurol.* **2019**, *32*, 100772. [[CrossRef](#)] [[PubMed](#)]
4. Manuck, T.A.; Rice, M.M.; Bailit, J.L.; Grobman, W.A.; Reddy, U.M.; Wapner, R.J.; Thorp, J.M.; Caritis, S.N.; Prasad, M.; Tita, A.T. Preterm neonatal morbidity and mortality by gestational age: A contemporary cohort. *Am. J. Obstet. Gynecol.* **2016**, *215*, e1–e103. [[CrossRef](#)] [[PubMed](#)]
5. Ophelders, D.R.; Gussenhoven, R.; Klein, L.; Jellema, R.K.; Westerlaken, R.J.; Hütten, M.C.; Vermeulen, J.; Wassink, G.; Gunn, A.J.; Wolfs, T.G. Preterm brain injury; antenatal triggers; therapeutics: Timing is key. *Cells* **2020**, *9*, 1871. [[CrossRef](#)] [[PubMed](#)]
6. Wachtel, E.V.; Verma, S.; Mally, P.V. Update on the current management of newborns with neonatal encephalopathy. *Curr. Probl. Pediatr. Adolesc. Health Care* **2019**, *49*, 100636. [[CrossRef](#)] [[PubMed](#)]
7. Gunn, A.I.; Drury, P.P. The pharmacology of hypothermia. In *Neonatal Neural Rescue: A Clinical Guide*; Cambridge University Press: Cambridge, UK, 2013; p. 73.
8. Thoresen, M.; Tooley, J.; Liu, X.; Jary, S.; Fleming, P.; Luyt, K.; Jain, A.; Cairns, P.; Harding, D.; Sabir, H. Time is brain: Starting therapeutic hypothermia within three hours after birth improves motor outcome in asphyxiated newborns. *Neonatology* **2013**, *104*, 228–233. [[CrossRef](#)] [[PubMed](#)]
9. Herrera, T.I.; Edwards, L.; Malcolm, W.F.; Smith, P.B.; Fisher, K.A.; Pizoli, C.; Gustafson, K.E.; Goldstein, R.F.; Cotten, C.M.; Goldberg, R.N. Outcomes of preterm infants treated with hypothermia for hypoxic-ischemic encephalopathy. *Early Hum. Dev.* **2018**, *125*, 1–7. [[CrossRef](#)] [[PubMed](#)]
10. Walsh, W.F.; Butler, D.; Schmidt, J.W. Report of a pilot study of cooling four preterm infants 32–35 weeks gestation with HIE. *J. Neonatal-Perinat. Med.* **2015**, *8*, 47–51. [[CrossRef](#)] [[PubMed](#)]
11. Abbasi, H.; Battin, M.R.; Butler, R.; Rowe, D.; Lear, B.A.; Gunn, A.J.; Bennet, L. Early signatures of brain injury in the preterm neonatal EEG. *Signals* **2023**, *4*, 630–643. [[CrossRef](#)]
12. Bennet, L.; Booth, L.; Gunn, A.J. Potential biomarkers for hypoxic-ischemic encephalopathy. *Semin. Fetal Neonatal Med.* **2010**, *15*, 253–260. [[CrossRef](#)] [[PubMed](#)]
13. Abbasi, H.; Drury, P.P.; Lear, C.A.; Gunn, A.J.; Davidson, J.O.; Bennet, L.; Unsworth, C.P. EEG sharp waves are a biomarker of striatal neuronal survival after hypoxia-ischemia in preterm fetal sheep. *Sci. Rep.* **2018**, *8*, 16312–16317. [[CrossRef](#)] [[PubMed](#)]
14. Abbasi, H.; Bennet, L.; Gunn, A.J.; Unsworth, C.P. Robust wavelet stabilized footprints of uncertainty for fuzzy system classifiers to automatically detect sharp waves in the EEG after hypoxia ischemia. *Int. J. Neural Syst.* **2017**, *27*, 1650051. [[CrossRef](#)] [[PubMed](#)]
15. Bennet, L.; Roelfsema, V.; Pathipati, P.; Quaedackers, J.S.; Gunn, A.J. Relationship between evolving epileptiform activity and delayed loss of mitochondrial activity after asphyxia measured by near-infrared spectroscopy in preterm fetal sheep. *J. Physiol.* **2006**, *572*, 141–154. [[CrossRef](#)] [[PubMed](#)]
16. Edwards, A.D.; Brocklehurst, P.; Gunn, A.J.; Halliday, H.; Juszczak, E.; Levene, M.; Strohm, B.; Thoresen, M.; Whitelaw, A.; Azzopardi, D. Neurological outcomes at 18 months of age after moderate hypothermia for perinatal hypoxic ischaemic encephalopathy: Synthesis and meta-analysis of trial data. *BMJ* **2010**, *340*, 409. [[CrossRef](#)] [[PubMed](#)]
17. Raurale, S.A.; Boylan, G.B.; Mathieson, S.R.; Marnane, W.P.; Lightbody, G.; O’Toole, J.M. Grading hypoxic-ischemic encephalopathy in neonatal EEG with convolutional neural networks and quadratic time-frequency distributions. *J. Neural Eng.* **2021**, *18*, 046007. [[CrossRef](#)] [[PubMed](#)]
18. Yu, S.; Marnane, W.P.; Boylan, G.B.; Lightbody, G. Neonatal hypoxic-ischemic encephalopathy grading from multi-channel EEG time-series data using a fully convolutional neural network. *Technologies* **2023**, *11*, 151. [[CrossRef](#)]
19. Gramacki, A.; Gramacki, J. A deep learning framework for epileptic seizure detection based on neonatal EEG signals. *Sci. Rep.* **2022**, *12*, 1–21. [[CrossRef](#)] [[PubMed](#)]
20. Raeisi, K.; Khazaei, M.; Croce, P.; Tamburro, G.; Comani, S.; Zappasodi, F. A graph convolutional neural network for the automated detection of seizures in the neonatal eeg. *Comput. Methods Programs Biomed.* **2022**, *222*, 106950. [[CrossRef](#)] [[PubMed](#)]
21. Tjepkema-Cloostermans, M.C.; de Carvalho, R.C.; van Putten, M.J. Deep learning for detection of focal epileptiform discharges from scalp EEG recordings. *Clin. Neurophysiol.* **2018**, *129*, 2191–2196. [[CrossRef](#)] [[PubMed](#)]
22. Deburchgraeve, W.; Cherian, P.J.; De Vos, M.; Swarte, R.M.; Blok, J.H.; Visser, G.H.; Govaert, P.; Van Huffel, S. Automated neonatal seizure detection mimicking a human observer reading EEG. *Clin. Neurophysiol.* **2008**, *119*, 2447–2454. [[CrossRef](#)] [[PubMed](#)]
23. Cherian, P.J.; Deburchgraeve, W.; Swarte, R.M.; De Vos, M.; Govaert, P.; Van Huffel, S.; Visser, G.H. Validation of a new automated neonatal seizure detection system: A clinician’s perspective. *Clin. Neurophysiol.* **2011**, *122*, 1490–1499. [[CrossRef](#)] [[PubMed](#)]
24. Tapani, K.T.; Vanhatalo, S.; Stevenson, N.J. Incorporating spike correlations into an SVM-based neonatal seizure detector. In *EMBECE & NBC 2017*; Anonymous; Springer: Berlin/Heidelberg, Germany, 2017; pp. 322–325.
25. Ansari, A.H.; Cherian, P.J.; Caicedo, A.; Dereymaeker, A.; Jansen, K.; De Wispelaere, L.; Dielman, C.; Vervisch, J.; Govaert, P.; De Vos, M. NeoGuard: A public, online learning platform for neonatal seizures. *arXiv* **2019**, arXiv:1905.12382.
26. Palmu, K.; Wikström, S.; Hippeläinen, E.; Boylan, G.; Hellström-Westas, L.; Vanhatalo, S. Detection of ‘EEG bursts’ in the early preterm EEG: Visual vs. automated detection. *Clin. Neurophysiol.* **2010**, *121*, 1015–1022. [[CrossRef](#)] [[PubMed](#)]
27. Abbasi, H.; Gunn, A.J.; Unsworth, C.P.; Bennet, L. Advanced deep learning spectroscopy of scalogram infused CNN classifiers for robust identification of Post-Hypoxic epileptiform EEG spikes. *Adv. Intell. Syst.* **2021**, *3*, 2000198. [[CrossRef](#)]
28. Abbasi, H.; Bennet, L.; Gunn, A.J.; Unsworth, C.P. 2D wavelet scalogram training of deep convolutional neural network for automatic identification of micro-scale sharp wave biomarkers in the hypoxic-ischemic EEG of preterm sheep. *Annu. Int. Conf. IEEE Eng. Med. Biol. Soc.* **2019**, *2019*, 1825–1828. [[PubMed](#)]

29. Selton, D.; Andre, M.; Hascoët, J.M. Normal EEG in very premature infants: Reference criteria. *Clin. Neurophysiol.* **2000**, *111*, 2116–2124. [[CrossRef](#)] [[PubMed](#)]
30. Vecchierini, M.; André, M.; d'Allest, A.M. Normal EEG of premature infants born between 24 and 30 weeks gestational age: Terminology, definitions and maturation aspects. *Neurophysiol. Clin./Clin. Neurophysiol.* **2007**, *37*, 311–323. [[CrossRef](#)] [[PubMed](#)]
31. Scher, M.S.; Hamid, M.Y.; Steppe, D.A.; Beggarly, M.E.; Painter, M.J. Ictal and interictal electrographic seizure durations in preterm and term neonates. *Epilepsia* **1993**, *34*, 284–288. [[CrossRef](#)]
32. Tyner, F.S.; Knott, J.R. *Fundamentals of EEG Technology: Basic Concepts and Methods*; Lippincott Williams & Wilkins: Philadelphia, PA, USA, 1983.
33. Tsuchida, T.N.; Wusthoff, C.J.; Shellhaas, R.A.; Abend, N.S.; Hahn, C.D.; Sullivan, J.E.; Nguyen, S.; Weinstein, S.; Scher, M.S.; Riviello, J.J.; et al. American clinical neurophysiology society standardized EEG terminology and categorization for the description of continuous EEG monitoring in neonates: Report of the american clinical neurophysiology society critical care monitoring committee. *J. Clin. Neurophysiol.* **2013**, *30*, 161–173. [[CrossRef](#)]
34. De Weerd, A.W.; Despland, P.A.; Plouin, P. Neonatal EEG. the international federation of clinical neurophysiology. *Electroencephalogr. Clin. Neurophysiol. Suppl.* **1999**, *52*, 149–157. [[PubMed](#)]
35. Abbasi, H.; Bennet, L.; Gunn, A.J.; Unsworth, C.P. Automatically identified micro-scale sharp-wave transients in the early-latent phase of hypoxic-ischemic EEG from preterm fetal sheep reveal timing relationship to subcortical neuronal survival. *Annu. Int. Conf. IEEE Eng. Med. Biol. Soc.* **2019**, *2019*, 7084–7087. [[PubMed](#)]
36. Kriegeskorte, N. Deep neural networks: A new framework for modeling biological vision and brain information processing. *Annu. Rev. Vis. Sci.* **2015**, *1*, 417–446. [[CrossRef](#)]
37. Shanmuganathan, S. *Artificial Neural Network Modelling: An Introduction*; Springer: Berlin/Heidelberg, Germany, 2016. Available online: [https://scholar.google.com/citations?view\\_op=view\\_citation&hl=en&user=i3qG2YcAAAAJ&citation\\_for\\_view=i3qG2YcAAAAJ:R22Rs3tN8aoC](https://scholar.google.com/citations?view_op=view_citation&hl=en&user=i3qG2YcAAAAJ&citation_for_view=i3qG2YcAAAAJ:R22Rs3tN8aoC) (accessed on 1 January 2024).
38. Zhang, J.; Yin, Z.; Chen, P.; Nichele, S. Emotion recognition using multi-modal data and machine learning techniques: A tutorial and review. *Inf. Fusion* **2020**, *59*, 103–126. [[CrossRef](#)]
39. Acharya, U.R.; Oh, S.L.; Hagiwara, Y.; Tan, J.H.; Adeli, H. Deep convolutional neural network for the automated detection and diagnosis of seizure using EEG signals. *Comput. Biol. Med.* **2018**, *100*, 270–278. [[CrossRef](#)] [[PubMed](#)]
40. Tozzi, A.; Peters, J.F.; Jausovec, N.; Don, A.P.; Ramanna, S.; Legchenkova, I.; Bormashenko, E. Nervous activity of the brain in five dimensions. *Biophysica* **2021**, *1*, 38–47. [[CrossRef](#)]
41. Pavel, A.M.; O'Toole, J.M.; Proietti, J.; Livingstone, V.; Mitra, S.; Marnane, W.P.; Finder, M.; Dempsey, E.M.; Murray, D.M.; Boylan, G.B. Machine learning for the early prediction of infants with electrographic seizures in neonatal hypoxic-ischemic encephalopathy. *Epilepsia* **2023**, *64*, 456–468. [[CrossRef](#)] [[PubMed](#)]
42. Gabeff, V.; Teijeiro, T.; Zapater, M.; Cammoun, L.; Rheims, S.; Ryvlin, P.; Atienza, D. Interpreting deep learning models for epileptic seizure detection on EEG signals. *Artif. Intell. Med.* **2021**, *117*, 102084. [[CrossRef](#)] [[PubMed](#)]
43. Rosas-Romero, R.; Guevara, E.; Peng, K.; Nguyen, D.K.; Lesage, F.; Pouliot, P.; Lima-Saad, W. Prediction of epileptic seizures with convolutional neural networks and functional near-infrared spectroscopy signals. *Comput. Biol. Med.* **2019**, *111*, 103355. [[CrossRef](#)]
44. Daftari, C.; Shah, J.; Shah, M. Detection of epileptic seizure disorder using EEG signals. In *Artificial Intelligence-Based Brain-Computer Interface*; Anonymous; Elsevier: Amsterdam, The Netherlands, 2022; pp. 163–188.
45. Nejedly, P.; Cimbalk, J.; Klimes, P.; Plesinger, F.; Halamek, J.; Kremen, V.; Viscor, I.; Brinkmann, B.H.; Pail, M.; Brazdil, M.; et al. Intracerebral EEG artifact identification using convolutional neural networks. *Neuroinformatics* **2019**, *17*, 225–234. [[CrossRef](#)] [[PubMed](#)]
46. Bahador, N.; Erikson, K.; Laurila, J.; Koskenkari, J.; Ala-Kokko, T.; Kortelainen, J. A correlation-driven mapping for deep learning application in detecting artifacts within the EEG. *J. Neural Eng.* **2020**, *17*, 056018. [[CrossRef](#)] [[PubMed](#)]
47. Lai, D.; Zhang, X.; Ma, K.; Chen, Z.; Chen, W.; Zhang, H.; Yuan, H.; Ding, L. Automated detection of high frequency oscillations in intracranial EEG using the combination of short-time energy and convolutional neural networks. *IEEE Access* **2019**, *7*, 82501–82511. [[CrossRef](#)]
48. Zuo, R.; Wei, J.; Li, X.; Li, C.; Zhao, C.; Ren, Z.; Liang, Y.; Geng, X.; Jiang, C.; Yang, X. Automated detection of high-frequency oscillations in epilepsy based on a convolutional neural network. *Front. Comput. Neurosci.* **2019**, *13*, 6. [[CrossRef](#)] [[PubMed](#)]
49. Wei, Z.; Zou, J.; Zhang, J.; Xu, J. Automatic epileptic EEG detection using convolutional neural network with improvements in time-domain. *Biomed. Signal Process. Control* **2019**, *53*, 101551. [[CrossRef](#)]
50. Zhou, M.; Tian, C.; Cao, R.; Wang, B.; Niu, Y.; Hu, T.; Guo, H.; Xiang, J. Epileptic seizure detection based on EEG signals and CNN. *Front. Neuroinformatics* **2018**, *12*, 95. [[CrossRef](#)]
51. Truong, N.D.; Nguyen, A.D.; Kuhlmann, L.; Bonyadi, M.R.; Yang, J.; Ippolito, S.; Kavehei, O. Integer convolutional neural network for seizure detection. *IEEE J. Emerg. Sel. Top. Circuits Syst.* **2018**, *8*, 849–857. [[CrossRef](#)]
52. O'Shea, A.; Lightbody, G.; Boylan, G.; Temko, A. Neonatal seizure detection from raw multi-channel EEG using a fully convolutional architecture. *Neural Netw.* **2020**, *123*, 12–25. [[CrossRef](#)] [[PubMed](#)]
53. Chakrabarti, S.; Swetapadma, A.; Pattnaik, P.K. A channel independent generalized seizure detection method for pediatric epileptic seizures. *Comput. Methods Programs Biomed.* **2021**, *209*, 106335. [[CrossRef](#)]

54. Yıldız, İ.; Garner, R.; Lai, M.; Duncan, D. Unsupervised seizure identification on EEG. *Comput. Methods Programs Biomed.* **2022**, *215*, 106604. [[CrossRef](#)] [[PubMed](#)]
55. Debelo, B.S.; Thamineni, B.L.; Dasari, H.K.; Dawud, A.A. Detection and severity identification of neonatal seizure using deep convolutional neural networks from multichannel EEG signal. *Pediatr. Health Med. Ther.* **2023**, *14*, 405–417. [[CrossRef](#)] [[PubMed](#)]
56. Tanveer, M.A.; Khan, M.J.; Sajid, H.; Naseer, N. Convolutional neural networks ensemble model for neonatal seizure detection. *J. Neurosci. Methods* **2021**, *358*, 109197. [[CrossRef](#)] [[PubMed](#)]
57. O’Shea, A.; Ahmed, R.; Lightbody, G.; Pavlidis, E.; Lloyd, R.; Pisani, F.; Marnane, W.; Mathieson, S.; Boylan, G.; Temko, A. Deep learning for EEG seizure detection in preterm infants. *Int. J. Neural Syst.* **2021**, *31*, 2150008. [[CrossRef](#)] [[PubMed](#)]
58. Ansari, A.H.; Cherian, P.J.; Caicedo, A.; Naulaers, G.; De Vos, M.; Van Huffel, S. Neonatal seizure detection using deep convolutional neural networks. *Int. J. Neural Syst.* **2019**, *29*, 4. [[CrossRef](#)] [[PubMed](#)]
59. Kota, S.; Jasti, K.; Liu, Y.; Liu, H.; Zhang, R.; Chalak, L. EEG spectral power: A proposed physiological biomarker to classify the hypoxic-ischemic encephalopathy severity in real time. *Pediatr. Neurol.* **2021**, *122*, 7–14. [[CrossRef](#)] [[PubMed](#)]
60. Bourel-Ponchel, E.; Querne, L.; Flamein, F.; Ghostine-Ramadan, G.; Wallois, F.; Lamblin, M.D. The prognostic value of neonatal conventional-EEG monitoring in hypoxic-ischemic encephalopathy during therapeutic hypothermia. *Dev. Med. Child Neurol.* **2023**, *65*, 58–66. [[CrossRef](#)] [[PubMed](#)]
61. Dereymaeker, A.; Matic, V.; Vervisch, J.; Cherian, P.J.; Ansari, A.H.; De Wel, O.; Govaert, P.; De Vos, M.; Van Huffel, S.; Naulaers, G. Automated EEG background analysis to identify neonates with hypoxic-ischemic encephalopathy treated with hypothermia at risk for adverse outcome: A pilot study. *Pediatr. Neonatol.* **2019**, *60*, 50–58. [[CrossRef](#)]
62. Moghadam, S.M.; Pinchefsky, E.; Tse, I.; Marchi, V.; Kohonen, J.; Kauppila, M.; Airaksinen, M.; Tapani, K.; Nevalainen, P.; Hahn, C. Building an open source classifier for the neonatal EEG background: A systematic feature-based approach from expert scoring to clinical visualization. *Front. Hum. Neurosci.* **2021**, *15*, 675154.
63. Duda, R.O.; Hart, P.E.; Stork, D.G. *Pattern Classification*; Wiley: Hoboken, NJ, USA, 2012.

**Disclaimer/Publisher’s Note:** The statements, opinions and data contained in all publications are solely those of the individual author(s) and contributor(s) and not of MDPI and/or the editor(s). MDPI and/or the editor(s) disclaim responsibility for any injury to people or property resulting from any ideas, methods, instructions or products referred to in the content.